The 20th International Flow Measurement Conference
FLOMEKO 2026

The Effect of Different Gases on Critical Flow Nozzles

J. D. Wright[1]*, C. J. Crowley[1], A. N. Johnson[1], and S. Nakao[2]

1 National Institute of Standards and Technology, Gaithersburg, MD, USA
2 Flow Col, Yokohama, Japan
* john.wright@nist.gov

Abstract

Critical nozzles and critical flow venturis are widely used gas flow meters because of their excellent calibration stability and well-developed flow theory. It is often desirable to calibrate them using one gas (dry air or nitrogen) and extrapolate that calibration to other gas species. The primary effects of gas species on the flow through critical nozzles are accounted for by the molar mass ($\mathcal{M}$) and the ideal gas critical flow function (C_I^*). Prior researchers derived how secondary gas species corrections enter through real gas effects, the inviscid core flow, the velocity and thermal boundary layers, and vibrational relaxation phenomena. This paper compares theoretical predictions of nozzle discharge coefficients to experimental measurements made using gases with specific heat ratios between 1.09 and 1.67, including some with vibrational relaxation effects (CO_2, SF_6, and N_2O) as large as 2.3 %. We introduce an approximate method for calculating the vibrational relaxation correction using an effective critical flow function $C_{\mathrm{I,eff}}^*$ that does not require a computational fluid dynamics simulation. For the cases examined, the agreement between experimental discharge coefficients and calculated values is better than 0.7 %.

1. Introduction

Critical flow venturis and critical nozzles are converging-diverging orifices with a large enough pressure difference across the smallest cross section (the throat) that the fluid attains the speed of sound. Specifications for the shape and usage of critical nozzles are given in the documentary standards ISO/DIS 9300 (2022) [1] and ASME MFC-7 (2016) [2]. Critical nozzles are widely used as gas flow meters because of their simplicity, low uncertainty and calibration stability (< 0.1 %), and well-developed theory of operation.

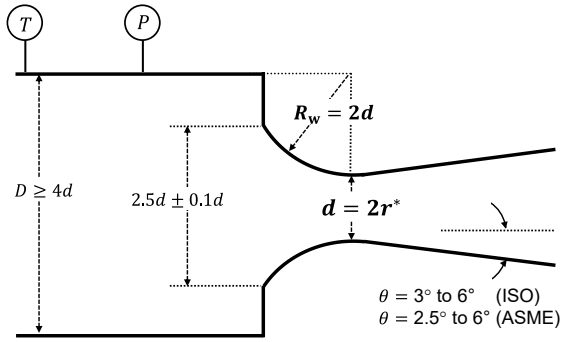

Figure 1. Geometry of a critical flow venturi as specified by ISO and ASME.

The primary effects of gas species on the mass flow ($\dot{m}$) through critical nozzles are accounted for by the molar mass ($\mathcal{M}$) and the ideal gas critical flow function (C_I^*):

$$\dot{m} = C_\mathrm{d}\, A^*\, C_\mathrm{I}^*\, P_0 \sqrt{\frac{\mathcal{M}}{\mathcal{R}\, T_0}} \qquad (1)$$

where $A^* = \pi d^{*2}/4$ is the area of the nozzle throat (* denotes throat value), P_0 and T_0 are the stagnation (or total) inlet pressure and temperature, $\mathcal{R} = 8.314462$ J / (mol K) is the universal gas constant, and C_d is the discharge coefficient that corrects errors in the ideal model. C_d is usually determined experimentally by calibration versus a flow reference, but it can also be calculated by combining several corrections [3]:

$$C_\mathrm{d} = C_\mathrm{real} C_\mathrm{inv} C_\mathrm{vbl} C_\mathrm{tbl} C_\mathrm{vib} C_\alpha \text{ , where} \qquad (2)$$

- C_real accounts for real gas effects and equals the ratio of the real [4] to ideal gas critical flow functions:

$$C_\mathrm{real} = \frac{C_\mathrm{R}^*}{C_\mathrm{I}^*} = \frac{C_\mathrm{R}^*}{\sqrt{\gamma_0 \left(\frac{2}{\gamma_0+1}\right)^{\frac{\gamma_0+1}{\gamma_0-1}}}} \quad , \qquad (3)$$

where $\gamma_0 = c_\mathrm{p}/c_\mathrm{V}$ is the specific heat ratio at P_0 and T_0.*

- C_inv accounts for 2-dimensional inviscid core flow effects [3],
- C_vbl corrects laminar [5] and turbulent velocity boundary layer effects with an adiabatic wall [3],

* Note that there are different versions of experimental C_d possible depending on which corrections are applied during the processing of experimental data. For example, an alternative version of Equation 1 could use C_R^* rather than C_I^* in which case the correction C_real in Equation 2 would be redundant.

- C_{tbl} accounts for thermal boundary layer effects resulting from heat transfer from the CFV wall to the flowing gas [6],
- C_{vib} corrects vibrational relaxation (thermodynamic non-equilibrium) effects [7, 8] and
- C_α accounts for the effects of thermal expansion on the diameter of the throat (d^*) [1]. C_α depends on the nozzle material and temperature and is independent of the gas species.

These corrections are defined relative to a baseline mass flow calculated via Equation 1 that was derived by assuming 1) 1-dimensional flow, 2) isentropic behavior (inviscid, adiabatic, and reversible), 3) ideal gas, and 4) constant γ.

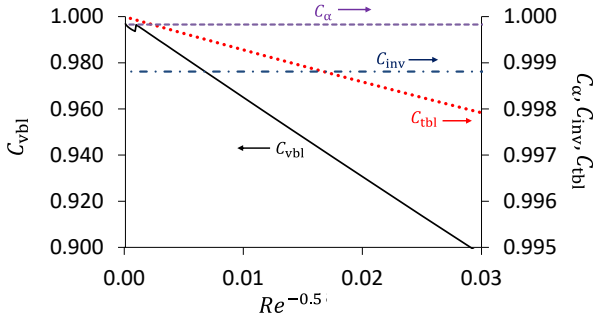

Figure 2: Critical nozzle corrections for Re = 1000 to ∞ for the conditions described in the text. C_{real} and C_{vib} are not shown but are significant for many gases and conditions.

Figure 2 shows the relative magnitudes of the correction factors versus the inverse square root of the Reynolds number $Re = \frac{4\dot{m}}{\pi d \mu_0}$, where μ_0 is the dynamic viscosity evaluated at the inlet conditions. The strong effect C_{vbl} is plotted on the left vertical axis which has scaling 20 × larger than the right axis where C_α, C_{inv}, and C_{tbl}, are plotted. The conditions used in **Figure 2** are:

1) standard nozzle geometry with normalized wall curvature $R_n = R_w/r^* = 4$ where R_w is the radius of curvature of the nozzle wall inlet and $r^* = d^*/2$,

2) the nozzle wall temperature T_w is 10 K hotter than the inlet gas temperature T_0,

3) real gas effects are negligible. Note that this is not the case, particularly for certain gases at high pressures, and

4) vibrational relaxation effects are negligible, *i.e.* the internal energy modes of the gas are in equilibrium. Note that this is often not the case for polyatomic gases like CO_2, SF_6, and N_2O (see Section 3).

C_{vbl} and C_{tbl} are proportional to the velocity and thermal boundary layer thicknesses, hence they are nearly linear when plotted versus $Re^{-0.5}$. The discontinuity in C_{vbl} near $Re^{-0.5} = 0.001$ is caused by boundary layer transition.

The cited literature on theory predicts C_d as a function of nozzle geometry, flow, temperatures, and gas properties allowing us to extrapolate a calibration performed in N_2 to usage in other gases. In this paper, we will compare theoretical and experimental values of C_d at $Re < 10^6$ (laminar boundary layers).

Section 2 shows the performance of the theoretical models for gases that do not have significant internal energy stored in vibrational modes at room temperature or that reach thermodynamic equilibrium rapidly.

Section 3 covers cases where vibrational relaxation effects are significant. For polyatomic molecules like CO_2, SF_6, and N_2O, the transit time from the nozzle inlet to the throat can be so rapid that the internal energy modes of the gas molecules remain partially "frozen" at the upstream conditions and using equilibrium values for thermodynamic quantities overpredicts the flow by 2 % or more.

2. Species effects from C_{inv}, C_{vbl}, and C_{tbl}

The derivation of the baseline nozzle flow model (Equation 1) assumes that flow in the nozzle is 1-dimensional when in fact inviscid momentum effects cause a curved sonic line near the throat. Solutions derived by Hall and by Kliegel and Levine [3] show that the necessary correction coefficient C_{inv} is a function of the normalized inlet wall curvature $R_n = R_w/r^*$ and the specific heat ratio γ.

Geropp's 1987 solution [6] for the non-adiabatic velocity and thermal boundary layers produces the corrections C_{vbl} and C_{tbl}. Geropp 1987 shows that the nozzle discharge depends on its geometry (d^* and R_n), the temperature ratio $(T_{wall} - T_0)/T_0$, and the gas properties γ, viscosity μ, and the Prandtl number $Pr = c_p\mu/k$ where k is thermal conductivity. Geropp 1987 simplifies to Geropp 1971 [5] for the adiabatic wall case ($T_{wall} = T_0$) and $Pr = 1$. How to calculate the inviscid core flow and boundary layer corrections is well explained elsewhere (*e.g.,* [3]) and will not be repeated here.

Publications by Nakao *et al.* [9], Nakao and Takamoto [10], Bobovnik *et al.* [11], and Wright [12] provide experimental measurements of C_d in 11 gases for 8 nozzles that can be compared to theoretical calculations. Other data sets are available but are not presented here because there was insufficient information to calculate C_d using the same database for property values.

Because species effects are most significant at low Reynolds numbers, the nozzles have small diameters and are difficult to manufacture to meet the ISO / ASME shape specifications. Hence, the geometric parameters d^* and R_n for each nozzle were adjusted from their nominal values so that the experimental measurements made with N_2 agreed well with theory: R_n changes the slope of C_d versus $Re^{-0.5}$ plots while d^* varies the zero intercept. Then those values of d^* and R_n were used to calculate theoretical C_d's for the other gas species. The geometric values and test gases for the 8 nozzles are listed in **Table 1**. The wide range of $R_n$values for the 8 nozzles means that the slopes of the C_d versus $Re^{-0.5}$ curves are quite different and would be confusing if plotted in the same figure.

Table 1. Parameters for the 8 nozzles used in the following data plots.

Source of data	Nominal d^* [mm]	Adjusted d^* [mm]	R_n	Gases
Nakao *et al.* [9]	0.5935	0.5929	4.1	N_2, O_2, Ar, He, C_2H_6, C_2H_4, CH_4, CO_2, SF6
Nakao and Takamoto [10]	0.295 1.1830 2.3580	0.2947 1.1838 2.3595	3.4 4.4 4.9	N_2, CO_2, SF6
Bobovnik *et al.* [11]	0.1750	0.1750	20	N_2, air, H_2, Ar, N_2O
Bobovnik *et al.* [11]	0.4360	0.4362	5.5	N_2, air, H_2, Ar, N_2O
Wright [12]	0.3937	0.3866	2.2	N_2, air, Ar, He, CO_2
Wright	0.2921	0.2853	0.5	N_2, Ar, He, CO_2

Figure 3 compares the experimental discharge coefficients $C_{d,\ expt}$ measured by Nakao *et al.* [9] to theoretical C_d values $C_{d,\ theo}$ calculated via Equation 2. All of the calculated theoretical C_d values in this section used the solutions of Kliegel and Levine for C_{inv} and Geropp '71 for C_{vbl} . The calculations assumed $Pr = 1$ and $(T_{wall} - T_0)/T_0 = 0$, so $C_{tbl} = 1$. Note that N_2, O_2, H_2, and air have nominal specific heat ratios of $\gamma \approx 1.4$, Ar and He have $\gamma \approx 1.67$, and that gases with similar specific heat ratios (same symbol shapes) are clustered together and in generally good agreement with theory (except for H_2). The theoretical values were calculated for the precise specific heat values for each gas and test condition, but the differences between the precise calculations and the generic lines shown in **Figure 3** would be imperceptible. The differences between theory and experiments are between 0.09 % and -0.13 % for N_2, O_2, and He. The Ar data have differences as large as -0.27 % and H_2 as large as 0.62 %. The expanded uncertainty of the Nakao *et al.* C_d measurements is 0.18 %.

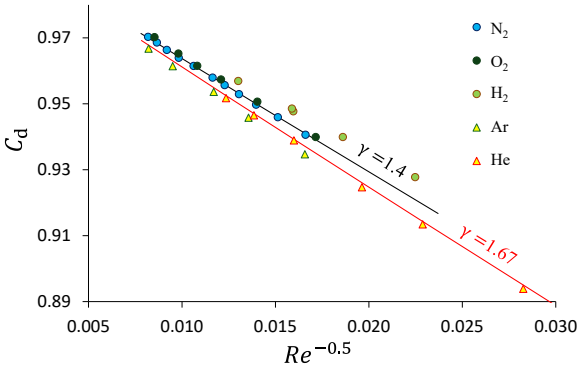

Figure 3: Experimental data from Nakao *et al.* [9] (symbols) and theoretical values (lines) of C_d plotted versus $Re^{-0.5}$ for gases that do not have significant vibrational relaxation effects at room temperature.

Surprisingly, using the more sophisticated Geropp 1987 solution, the actual Prandtl numbers for each gas ($Pr \neq 1$), and $(T_{wall} - T_0)/T_0 = 0$ worsens the agreement between experimental and theoretical results. The disagreement between calculated and experimental values approximately doubles for the gases with $\gamma \neq 1.4$ (the value for N_2, the gas used to fit the geometric parameters). This is due to thermal boundary layer effects and the adiabatic wall assumption. When $Pr = 1$, the recovery factor $R_f = \sqrt{Pr} = 1$ and the wall temperature matches the inlet gas temperature T_0. For $Pr < 1$, $T_{wall} < T_0$, especially for gases with high γ like He and Ar. Colder T_{wall} causes increased mass flux in the boundary layer and higher theoretical C_d values. But in real nozzle applications using a conductive metal nozzle body material like stainless steel, the wall temperature remains close to the inlet and room temperature, especially for small Reynolds numbers where boundary layer effects are most significant. Hence the assumption $Pr = 1$ and $(T_{wall} - T_0)/T_0 = 0$ in the simpler Geropp '71 and Tang models produce better agreement with experiments than the more sophisticated Geropp 1987 model. Perhaps using the theory of Geropp 1987 along with nozzles equipped with sensors to measure T_{wall} would produce even better results than shown in **Figure 3** and the following plots comparing experimental and theoretical C_d's.

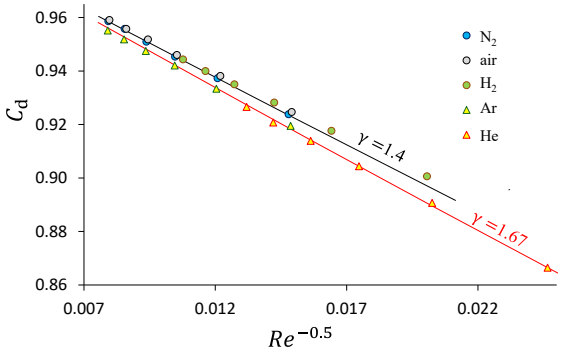

Figure 4: Experimental data from Bobovnik *et al.* [11] for $d = 0.1750$ mm (points) and theoretical values (lines) of C_d plotted versus $Re^{-0.5}$ for gases that do not have significant energy in their vibrational modes at room temperature.

Experimental results from Bobovnik *et al.* [11] for the nozzle with $d^* = 0.175$ mm are plotted along with theoretical C_d values in **Figure 4**. The agreement between theory and experiment is better than 0.2 % except for H_2, for which experimental results are higher than theory by as much as 0.41 % (similar to the results of Nakao *et al.*). The expanded uncertainty of the Bobovnik *et al.* C_d measurements is 0.17 %.

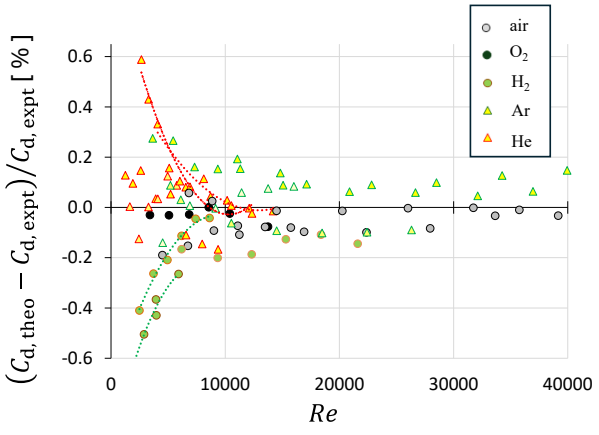

Figure 5: Difference between the theoretical and experimental C_d values for nozzles listed in **Table 1** and for gases that do not have significant vibrational relaxation effects.

The difference between the experimental and theoretical C_d values for 5 nozzles is plotted in **Figure 5**. Due to fitting of geometric parameters, the differences for N_2 are nearly zero so they are not plotted to reduce clutter. The differences in **Figure 5** are generally less than 0.15 %, less than the uncertainty of the experimental measurements. Four data sets, marked with 2nd order polynomial curves, fall outside that limit at $Re < 10^4$, and we make the following observations: He data measured by Bobovnik *et al.* and Wright are lower than theory predicts while H_2 data measured by Nakao *et al.* and Bobovnik *et al.* are higher. The explanation for these trends, observed in different laboratories, is not known, but they could be related to leaks which are difficult to eliminate for He and H_2. Also, the large differences happen at low Reynolds numbers where velocity and thermal boundary layer effects are strongest. It seems unlikely that the poor agreement for H_2 is caused by thermodynamic differences between the ortho and para hydrogen spin states: while their heat capacities differ significantly, their proportions were likely in equilibrium and unchanging during these experiments.

3. Vibrational relaxation effects

In the absence of molecular disassociation and chemical reactions, the internal energy of a set of gas molecules is distributed between three types of motion: translation, rotation, and vibration that are illustrated in **Figure 6** for diatomic nitrogen. When a gas undergoes a change in temperature, the energy stored in the three modes undergoes a change via molecular collisions. The number of collisions necessary to equilibrate the vibrational modes is larger than for the translational and rotational modes since the vibrational phases of two colliding molecules need to match during the collision in order to efficiently transfer energy. This leads to a longer equilibration (relaxation) time for the vibrational modes τ_{vib}, as compared to the translational and rotational modes.

If the residence time $\tau_{\text{res}} = \int_{x_0}^{x_1} dx/u(x)$ for a gas molecule to move from the nozzle inlet to the throat is comparable to or faster than τ_{vib}, the vibrational modes will be out of equilibrium with the translational and rotational modes of the gas. A consequence of the vibrational modes being out of equilibrium with the other modes is that the internal energy is not simply proportional to temperature as given by the equipartition theorem; therefore, γ is not well defined and approximations are needed. For the ISO / ASME nozzle geometry (see **Figure 1**) with a 0.5 mm diameter, the residence time is approximately 10 µs, which is comparable to the vibrational relaxation time for some gases. The vibrational relaxation time depends on the specifics of the molecule and the gas temperature and pressure, which here is modeled as the temperature derived only from the translational and rotational modes. This model assumes the vibrational modes are a thermodynamic subsystem at temperature T_{vib} in thermal contact with the reservoir of translational and rotational modes at temperature $T_{\text{trans + rot}} = T$. This framework gives rise to the Landau-Teller relaxation law for vibrational energy along a streamline [13]:

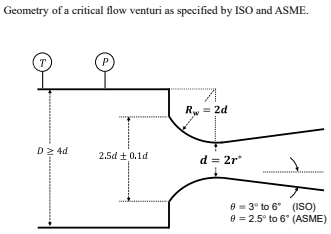

$$\frac{d\epsilon_{\text{vib}}(T_{\text{vib}})}{dx} = \frac{\epsilon_{\text{vib}}(T) - \epsilon_{\text{vib}}(T_{\text{vib}})}{u(x)\,\tau_{\text{vib}}}, \qquad (4)$$

where $u(x)$ is the gas speed at axial position x.

The effect of non-equilibrium vibrational modes on the flow depends on the fraction of the internal energy stored in the vibrational modes compared to the translation and rotational modes. If there is nearly no energy in the vibrational modes, there will be nearly no effect on the flow physics. The energy stored in each mode depends on the structure of the molecule, *e.g.*, a monatomic gas like He has no vibrational mode while complex polyatomic molecules can have significant vibrational energy. Some polyatomic gases hold significant portions of their internal energy in the vibrational modes at room temperature, *e.g.*, $\epsilon_{\text{vib}}/\epsilon \approx 10$ % for CO_2 and N_2O and 50 % for SF_6.

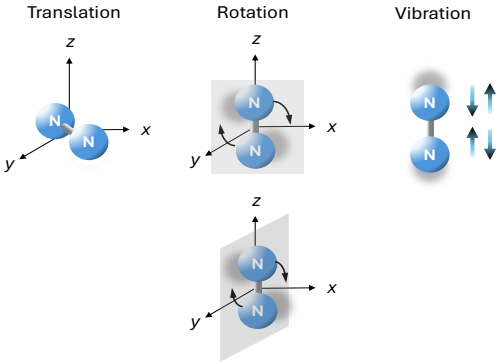

Figure 6: Schematic representation of the three modes of molecular motion for a diatomic molecule.

Two conditions lead to vibrational relaxation effects in critical nozzles:

1) The time constant for vibrational energy redistribution with the translational and rotational modes τ_{vib} is comparable to the flow residence time, *i.e.*, $\tau_{\text{vib}} \gtrsim \tau_{\text{res}}$ and
2) Vibrational energy makes a significant contribution to the total internal energy of the gas, *i.e.*, $\epsilon_{\text{vib}}/\epsilon > 0$. Simpler molecules (*e.g.*, N_2, H_2, and O_2) relax slowly, but do not have sufficient vibrational energy at the typical nozzle operating temperatures for relaxation effects to be important. However, larger polyatomic molecules do (*e.g.*, CO_2, SF_6, N_2O, CH_4).

4. Correcting Vibrational Relaxation Effects, C_{vib}

Uncorrected vibrational relaxation effects cause higher than expected experimental values for the discharge coefficient, by 2 % or more for some gases and nozzle sizes. Explanations and approaches for correcting vibrational relaxation effects in critical nozzles were independently developed by Babiano [7] and Johnson [8, 14]. Johnson's computer simulations that included relaxation effects for CO_2 and SF_6 produced discharge coefficients that agreed with Nakao's [9] experimental measurements within 0.5 %. Johnson's simulations capture vibrational relaxation effects by solving the Landau-Teller vibrational rate equation simultaneously with the mass, momentum, and energy conservation equations.

Now we present an approximate method to calculate a vibrational relaxation discharge correction C_{vib} based on Babiano's and Johnson's model. By definition, C_{vib} is the ratio of the mass flow when the gas vibrational temperature is in its non-equilibrium state to the mass flow when the vibrational temperature is in equilibrium with the external (translational and rotational) temperature T. C_{vib} can be calculated via an effective specific heat ratio γ^*_{eff} for the partially frozen flow that differs from the equilibrium value at the throat γ^*:

$$C_{\mathrm{vib}} = \frac{\dot{m}_{\mathrm{vib}}}{\dot{m}_{\mathrm{eq}}} = \frac{C^*_{\mathrm{I\,eff}}}{C^*_{\mathrm{I\,eq}}} = \frac{\sqrt{\gamma^*_{\mathrm{eff}}\left(\frac{2}{\gamma^*_{\mathrm{eff}}+1}\right)^{\frac{\gamma^*_{\mathrm{eff}}+1}{\gamma^*_{\mathrm{eff}}-1}}}}{\sqrt{\gamma^*\left(\frac{2}{\gamma^*+1}\right)^{\frac{\gamma^*+1}{\gamma^*-1}}}} \quad . \tag{5}$$

Here, C^*_{I} is the ideal critical flow function with subscripts "eq" and "eff" to indicate values of C^*_{I} that are calculated from equilibrium values of the specific heat ratio at the throat γ^* or partially frozen values γ^*_{eff}.

The process for numerically calculating γ^*_{eff} is:

Use the subsonic branch of the isentropic area-Mach relation to calculate the area ratios that correspond to $N \geq 90$ equally spaced Mach number M values between 0 and 1, the value at the nozzle throat:

$$\frac{A(x)}{A^*} = \frac{1}{M(x)}\left[\frac{2}{\gamma_0+1}\left(1+\frac{\gamma_0-1}{2}M(x)^2\right)\right]^{\frac{\gamma_0+1}{2(\gamma_0-1)}} \quad . \tag{6}$$

Here, x is the axial position and γ_0 is the specific heat ratio for the inlet stagnation conditions. The axial positions associated with those area ratios (with $x = 0$ at the throat) are:

$$x = -r^*\,R_{\mathrm{n}}\cos\left(\sin^{-1}\left\{1+\left[r^*\left(1-\sqrt{\frac{A(x)}{A^*}}\right)/R_{\mathrm{n}}\right]\right\}\right). \tag{7}$$

Then calculate the static temperature, pressure, and speed at each axial position using the equations for an isentropic one-dimensional flow of a perfect gas:

$$T(x) = \frac{T_0}{1+\frac{\gamma_0-1}{2}M(x)^2} \quad , \tag{8}$$

$$p(x) = \frac{p_0}{\left[1+\frac{(\gamma_0-1)}{2}M(x)^2\right]^{\frac{\gamma_0}{\gamma_0-1}}} \quad \text{, and} \tag{9}$$

$$u(x) = M(x)\sqrt{\gamma_0\left(\frac{\mathcal{R}}{\mathcal{M}}\right)T(x)} \quad . \tag{10}$$

The relationship between the fast-evolving external temperature T and the vibrational temperature T_{vib} can be calculated along a streamline at speed $u(x)$ by a backward-Euler numerical integration of the Landau-Teller equation (Equation 4) over the N axial positions. Assume equilibrium as the initial condition at the nozzle inlet, *i.e.* $T_{\mathrm{vib}} = T$ at $i = 0$. The vibrational internal energy at steps i =1 to N is:

$$\epsilon_{\mathrm{vib}}\left(T_{\mathrm{vib}_i}\right) = \frac{\epsilon_{\mathrm{vib}}\left(T_{\mathrm{vib}_{i-1}}\right)+\lambda_i\epsilon_{\mathrm{vib}}(T_i)}{1+\lambda_i} \text{ , where} \tag{11}$$

$$\lambda_i = \frac{(x_i - x_{i-1})}{u_i\,\tau_{\mathrm{vib}_i}} \quad . \tag{12}$$

The vibrational time constant depends on the pressure, the temperature, which vibrational modes exist, and which modes are energetic for the particular gas species. An empirical equation for the vibrational time constant is [13]:

$$\tau_{\mathrm{vib}} = K_1\,\frac{\exp\left[(K_2/T)^{1/3}\right]}{p} \, . \tag{13}$$

A gas that is hotter and denser gas has a smaller time constant and relaxes to equilibrium faster. The coefficients K_1 and K_2 for gases studied in this paper are listed in **Table 2**.

Table 2. Coefficients for the vibrational relaxation time constant of gases studied in this paper [14, 15, 16, 17].

Gas	K_1 (Pa-s)	K_2 (K)
CO_2	0.0420	10635
SF_6	0.0589	0
N_2O	0.0024	15379
CH_4	0.0043	9352
C_2H_2	0.0003	11080
C_2H_6	0.0011	0

The vibrational internal energy ϵ_{vib} can be calculated via equations using the vibrational mode degeneracies and characteristic temperatures [13, 18] or from REFPROP [4].*

The effective heat capacity at the throat is:

$$c^*_{\mathrm{v\,eff}} = \varphi\,\mathcal{R} + \frac{\epsilon_{\mathrm{vib}N}-\epsilon_{\mathrm{vib}N-1}}{T_N - T_{N-1}} \quad , \tag{14}$$

where φ is the number of translational and rotational modes divided by 2 and is equal to 2.5 for linear

* To calculate C_{vib} via REFPROP, use the ideal-gas commands "CV0" and "E0" to eliminate real gas effects. It is also necessary to subtract the rotational and translational contributions and an arbitrary offset that is included in the REFPROP internal energies, *i.e.* $\epsilon_{\mathrm{vib}}(T) = \epsilon(T) - \varphi\,\mathcal{R}(T - T_{\mathrm{ref}}) - \epsilon(T_{\mathrm{ref}})$ where T_{ref} is a reference temperature cold enough (*e.g.* T_{ref} = 200 K) that vibrational modes are not excited.

molecules (*e.g.*, CO_2, N_2O, and C_2H_2) and equal to 3 for non-linear molecules (*e.g.*, SF_6 and CH_4).

For an ideal gas, the effective heat capacity ratio at the throat is:

$$\gamma^*_{\text{eff}} = \frac{c^*_{\text{v eff}} + \mathcal{R}}{c^*_{\text{v eff}}} \quad . \tag{15}$$

With the values of γ^*_{eff} and the equilibrium value of γ^* in hand, C_{vib} can be calculated using Equation 5. Note that γ^*_{eff} applies at the nozzle throat and that the equilibrium value of γ^* also must be for the throat conditions p^* and T^* so that $C_{\text{vib}} = 1$ when $T^*_{\text{vib}} = T^*$. This is counter-intuitive because the equation for C^*_{I} is derived partially to account for the isentropic evolution of temperature and pressure between the stagnation and throat conditions. But it is necessary to use an equilibrium value for γ^* calculated from Equation 15 and $c_{\text{V}}(p^*, T^*_{\text{vib}})$ to properly normalize the $C^*_{\text{I eff}}$.

Figure 7 plots T and T_{vib} versus the streamwise position calculated by the methods described herein for CO_2 and SF_6, $p_0 = 50$ kPa, $T_0 = 300$ K, $d^* = 0.5929$ mm and $R_{\text{n}} = 4.1$. For CO_2, the vibrational energy is nearly completely frozen (relaxed fraction at the throat $\text{d}T^*_{\text{vib}}/\text{d}T^* \approx 0$) and $T^*_{\text{vib}} = 298.15$ K is nearly equal to the inlet temperature. For SF_6, $\text{d}T^*_{\text{vib}}/\text{d}T^* = 0.41$.

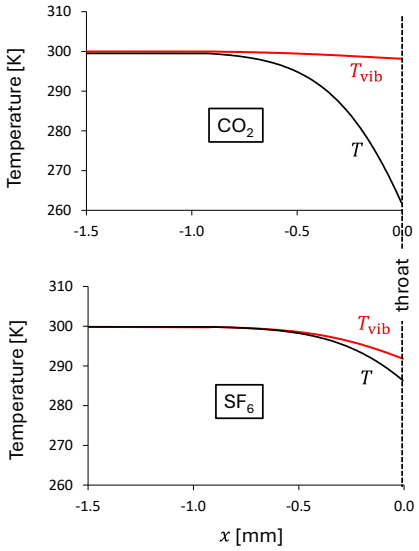

Figure 7. Plots of equilibrium and vibrational temperatures versus streamwise position for CO_2 and SF_6.

Experimental measurements by Nakao and theoretical C_{d} values calculated by the method described above are plotted in **Figure 8**.

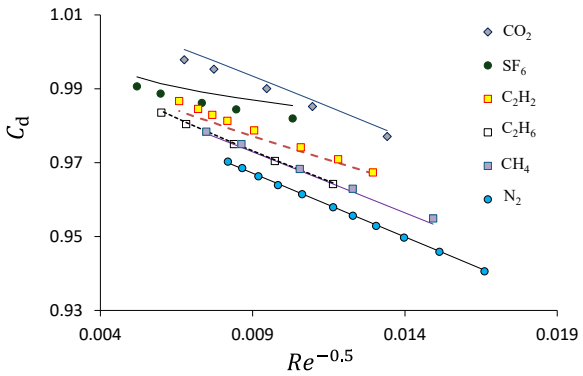

Figure 8. Experimental results of Nakao *et al.* for $d^* = 0.5929$ mm plotted versus the theoretical C_{d} values for gases with significant vibrational relaxation effects. Nitrogen (no relaxation effects) is shown for reference.

Figure 9 shows the improvement in C_{d} values that results when C_{vib} is applied to all the available experimental measurements listed in **Table 1**. The maximum differences are reduced from -2.3 % to 0.7 %. The theoretical C_{vib} values are generally high relative to experimental ones, *i.e.* the calculated relaxed fraction is too low. This can be due to using too long τ_{vib} or errors introduced by assumptions in the calculation method.

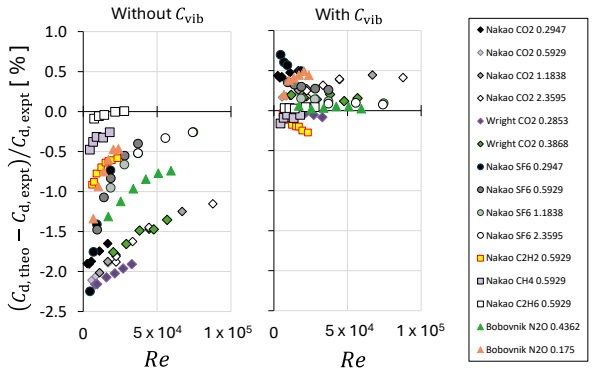

Figure 9. A comparison of experimental and calculated C_{d} values with and without application of C_{vib}. The legend lists the data source, gas, and d^* in mm.

5. Conclusions

A goal of this work was to use available experimental data to assess the ability of theory to predict species effects in critical nozzles. **Figures 5** and **9** present the results for gases with and without significant vibrational relaxation effects.

A second goal was to develop an engineering approximation to calculate C_{vib} that would avoid the need for a full computational fluid dynamics simulation. The method in Section 4 allows nozzle users to estimate or correct relaxation effects more easily. We plan to follow up this work by computing exact numerical solutions for C_{vib} based on one-dimensional flow of perfect gas not in vibrational equilibrium. This will allow us to directly assess the accuracy of our approximate model.

We found that the theoretical calculations of C_{vib} generally overestimate the vibrational effects. This may be because of our assumption of a constant specific heat

ratio in the area-Mach number relations or values of τ_{vib} that are too large.

Other topics warranting further investigation are:

- The possibility of a further simplification of the engineering approximation for a particular nozzle geometry based on the ratio of $\tau_{\mathrm{vib}}/\tau_{\mathrm{res}}$.
- Why experimental discharge coefficients for He and H_2 depart from theory at low Reynolds numbers.

Acknowledgements: ChatGPT v. 5.2 and Claude were used during the preparation of this paper.

References

[1] International Standards Organization, *Measurement of Gas Flow by Means of Critical Flow Venturi Nozzles*, ISO 9300, 3rd edition, 2022.

[2] American Society of Mechanical Engineers, *Measurement of Gas Flow by Means of Critical Flow Venturis and Critical Flow Nozzles*, ASME MFC-7-2016.

[3] Johnson, A. N. and Wright, J. D., *Comparison between Theoretical CFV Models and NIST's Primary Flow Data in the Laminar, Turbulent, and Transition Flow Regimes*, ASME Journal of Fluids Engineering, vol. 130, July, 2008.

[4] Lemmon, E. W., Bell, I. H., Huber, M. L., and McLinden, M. O., *NIST Standard Reference Database: Reference Fluid Thermodynamic and Transport Properties-REFPROP*, Version 10.0, National Institute of Standards and Technology, Standard Reference Data Program, Gaithersburg, 2018.

[5] Geropp, D., *Laminare Grenzschichten in Ebenen und Rotationssymmetrischen Lavaldüsen*, Deutsche Luft- und Raumfahrt, Forschungsbericht 71 – 90, 1971.

[6] Geropp, D., *Grenzschichten in Überschalldüsen*, Deutsche Luft- und Raumfahrt Forschungsbericht 01 TM 8603-AK/PA 1, November 1987.

[7] Babiano, A., I*nfluence de la Relaxation de Vibration sur un Ecoulement Gazeux en Tuyere*, Acta Astronautica, Volume 2, Issues 5- May-June, pp. 431 – 443, 1975.

[8] Johnson, A. N., Merkle. C. L., Moldover, M. R., and Wright, J. D., *Relaxation Effects in Small Critical Nozzles*, ASME J. of Fluids Engineering, 128, pp. 170-176, 2006.

[9] Nakao, S., Hirayama, T., Yokoi, Y., and Takamoto, M., *Effects of Thermophysical Properties of Gases on the Discharge Coefficients of the Sonic Venturi Nozzle*, FEDSM97-3005, Proceedings of the ASME Fluids Engineering Summer Meeting, Vancouver, Canada, 1997.

[10] Nakao, S. and Takamoto, M., D*ischarge Coefficients of Critical Venturi Nozzles for CO_2 and SF_6*, ASME Journal of Fluids Engineering, 122, pp. 730 to 734, 2000.

[11] Bobovnik, G., Mickan, B., Sambol, P., Maury, R., and Kutin, J., *Investigation of the Discharge Coefficient in the Laminar Boundary Layer Regime of Critical Flow Venturi Nozzles Calibrated with Different Gases Including Hydrogen*, Measurement, 217, 2023.

[12] Wright, J. D., *What is the "Best" Transfer Standard for Gas Flow?*, Proceedings of FLOMEKO, Groningen, Netherlands, 2003.

[13] Vincenti, W. G. and Kruger, C. H., *Introduction to Physical Gas Dynamics*, John Wiley and Sons, 1965.

[14] Johnson, A. N., *Numerical Characterization of the Discharge Coefficient in Critical Nozzles*, Ph.D. Thesis, Pennsylvania State Univ., University Park, Pennsylvania, USA, 2000.

[15] O'Conner, L. C., *Thermal Relaxation of Vibrational States in Sulfur Hexafluoride*, J. Acoust. Soc. Am., 26, pp. 361-364, 1954.

[16] Simpson, C. J., S. M., Gait, P. D., Price, T. J., and Foster, M. G., *A Shock Tube Study of Vibrational Relaxation in Pure N_2O and Mixtures of N_2O with Argon, Helium-4, Helium-3, Deuterium, Hydrogen Deuteride, Normal, and Para-Hydrog*en, Chemical Physics, 68, pp. 293 to 302, 1982.

[17] Wang, J. C. F. and Springer, G. S., *Vibrational Relaxation Times in Some Hydrocarbons in the Range 300 – 900 K*, J. Chem. Phys., 59, pp. 6556 to 6562, 1973.

[18] Johnson, R. D. III**,** NIST Computational Chemistry Comparison and Benchmark Database, *NIST Standard Reference Database Number 101*, National Institute of Standards and Technology, Gaithersburg, MD (2002), DOI:10.18434/T47C7Z
Available at: https://cccbdb.nist.gov/introx.asp